International Forum on Aeroelasticity and Structural Dynamics
IFASD 2019
9-13 June 2019, Savannah, Georgia, USA

VERY FLEXIBLE AIRCRAFT CONTROL BASED ON LOOP-SEPARATION AND REFERENCE GOVERNOR

Pedro J. González[1], Mateus de Freitas Virgilio Pereira[2], Flávio J. Silvestre[3], Ilya Kolmanovsky[2], and Carlos E. S. Cesnik[2]

[1]Instituto Tecnológico de Aeronáutica
São José dos Campos, SP, 12228-900, Brazil
pedrojgonzalezr@gmail.com

[2]University of Michigan
Ann Arbor, Michigan, 48109-2140, USA
mfvp@umich.edu
ilya@umich.edu
cesnik@umich.edu

[3]Technische Universität Berlin
Marchstrasse 12, 10587 Berlin, Germany
flavio.silvestre@tu-berlin.de

Keywords: aeroservoelasticity, control of flexible aircraft, reference governor, loop-separation, model predictive control

Abstract: To handle more complex dynamic behavior due to high-aspect-ratio wings in very flexible aircraft, more complex models and control methods are needed. In this paper, a control approach is proposed which combines a loop-separation architecture with inner and outer loops and a reference governor that acts as a safety supervisor for reference inputs to the autopilot. While the inner-loop is capable of controlling the shape of the aircraft and providing stability, the outer-loop ensures tracking of velocity, altitude, bank and heading angles. The reference governor complements this architecture and protects the system against constraint violations. The modularity of this approach facilitates the practical implementation of this control architecture.

1 INTRODUCTION

The Loop-Separation Control (LSC) has been proposed in [1], [2] for control of very flexible aircraft (VFA). In the LSC, the inner-loop is in charge of stabilizing the aircraft by decoupling longitudinal and lateral-directional dynamics. The outer-loop in LSC is designed to track velocity, altitude, sideslip and heading angles based on structured H_∞-synthesis algorithms. The latter technique allows designing controllers with fixed structure (form or dimensions), resulting in simpler controllers with the desired input-output coupling and avoiding the large online computational requirements associated with H_∞ controllers designed based on the high order models [3]. At the same time, structured H_∞ synthesis still provides the flexibility to formulate and handle control requirements as in the regular H_∞ theory. These requirements are addressed in the outer-loop optimization process as constraints on phase and gain margins, shape of sensitivity and complementary sensitivity functions and locations of the closed-loop system poles. In [1], it was shown that the LSC architecture is capable of achieving good control performance

with low steady state error and good noise rejection for flexible aircraft. Further studies showed it to be capable of operating aircraft under hazardous weather conditions (turbulent/high-gust profiles). Nevertheless, the LSC by itself is not able to enforce the constraints when the maneuvers are tighter or closer to the aircraft operational limits (maximum sideslip angle or stall speed). To avoid constraint violation and to ensure safe aircraft operation, in this paper a reference governor is proposed as an augmentation to the LSC architecture.

A reference governor (RG) is an add-on control scheme to a nominal closed-loop system [4] which monitors and supervises commands/references to protect against constraint violations. In this work, the reference governor is designed using Model Predictive Control (MPC) [4]. The main advantage of using RG is the capability of preserving the characteristics of an existing controller whenever there is no danger of constraint violation. This avoids the task of redesigning and replacing a well tuned controller. This approach also preserves the modularity of the LSC.

In the present work, the capabilities and advantages of the LSC assisted by the RG are evaluated and analyzed for the X-HALE VFA. Nonlinear simulation results using University of Michigan's Nonlinear Aeroelastic Simulation Toolbox (UM/NAST) ([5], [6]) high fidelity modeling environment highlight the improvements in control provided by the RG.

2 MODEL DESCRIPTION AND CONTROL SYSTEM STRUCTURE

The X-HALE is a radio-controlled very flexible aircraft [7]. The version of the aircraft considered in this paper has 6 m wingspan and a constant wing chord of 0.2 m. Figure 1 shows a picture of the aircraft. The five pods distributed equidistantly on the wing carry the motors (F_0, F_1, F_2, F_3, F_4, F_5) and the instrumentation. Five tail booms are attached to these spines holding the stabilizers (δ_{ro}, δ_{ri}, δ_{F0}, δ_{li}, δ_{lo}). The external wing panels have a dihedral installation angle of 10 deg, and spoilers (δ_{rs}, δ_{ls}) installed on them. This vehicle was designed to gather data to validate nonlinear aeroelastic-coupled-flight mechanics codes and flight control laws.

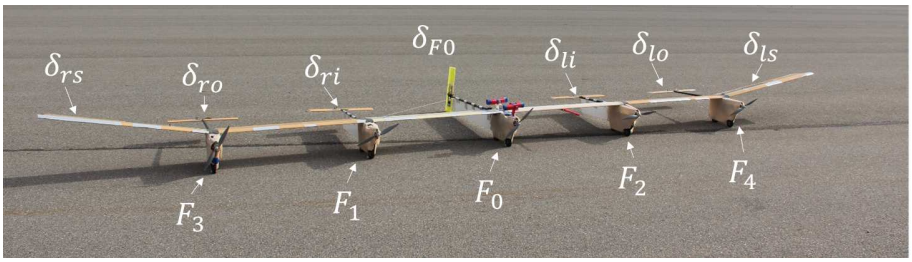

Figure 1: X-HALE geometry and control surfaces.

The aircraft was modeled in UM/NAST [5], [6]. A reduced order linearized model with 60 states extracted from UM/NAST was used for controller design. The open-loop simulations showed very good agreement with the full order model that has 344 states. The state vector is defined as

$$x = \begin{bmatrix} \varepsilon^T & \dot{\varepsilon}^T & \beta_m^T & \zeta^T & P_G^T \end{bmatrix}^T, \tag{1}$$

where the notations are further explained in what follows.

Each wing panel is modeled using a single nonlinear beam element. Each element i is defined by four states:

$$\varepsilon_i = \left[\epsilon_{yy,i},\ \kappa_{x,i},\ \kappa_{y,i},\ \kappa_{z,i} \right]^T, \tag{2}$$

which are the axial strain $\epsilon_{yy,i}$ and three orthogonal curvatures, $\kappa_{x,i}$, $\kappa_{y,i}$ and $\kappa_{z,i}$. In the body-fixed frame, x is chordwise, y is in the direction of the wing span and z completes the axes pointing upwards. The model includes forty-eight states for the structures dynamics. Thirteen states represent the rigid body dynamics of the aircraft. Six of these are aggregated into a vector β_m which comprises linear velocities $\bar{u}$, $\bar{v}$,$\bar{w}$, and the angular velocities for roll (p), pitch (q) and yaw (r). The vector ζ contains quaternions q_0, q_1, q_2 and q_3 used to represent the orientation of the vehicle. The vector P_G contains the inertial position, in which the vertical displacement is the altitude (h).

The coupled nonlinear aeroelastic and rigid body equations of motion have the following general form:

$$M(q)\ddot{q} + C(q,\dot{q})\dot{q} + Kq = R(q,\dot{q},\zeta,u), \tag{3}$$

while the body-fixed reference frame propagation equations are

$$\dot{\zeta} = -\frac{1}{2}\Omega(\beta_m)\zeta, \tag{4}$$

$$\dot{P}_G = \left[\begin{array}{cc} C^{GB} & 0_{3\times 3} \end{array} \right] \beta_m, \tag{5}$$

where $q = \left[\begin{array}{cc} \epsilon^T & b^T \end{array} \right]^T$, b is vector that aggregates position and orientation, u is the control input, $M(q)$ is the generalized mass matrix, $C(q,\dot{q})$ is the generalized damping matrix, K is the generalized stiffness matrix, $R(q,\dot{q},\zeta,u)$ is the state-dependent generalized force vector, $\Omega(\beta_m)$ is the matrix for propagating the first-order quaternion differential equations, and C^{GB} is the transformation matrix from the body-fixed frame to the inertial frame.

While the nonlinear Eqs. 3-5 are used for simulation in the UM/NAST environment, the control architecture proposed in this paper is based on linearized models. Futhermore, Euler angles are used in lieu of quartenions for control design. The angles ϕ, θ and ψ are the roll, pitch and heading angles, respectively. Hence, Eqs. 3-5 are linearized about the typical X-HALE cruise flight condition at 30 m and 14 m/s, yielding a continuous-time linear model of form:

$$\dot{x} = Ax + Bu, \tag{6}$$

$$y = Cx + Du, \tag{7}$$

with state vector given by Eq. 1. Note that the variables x and u in Eq. 6 denote variations from the trim condition.

The total velocity (V) is the module of all linear velocities. The linear velocities and the total velocity are also used to calculate the angle of attack (α) and the sideslip angle (β) in the output matrix.

$$\alpha = \arctan\left(\frac{\bar{w}}{\bar{u}}\right), \beta = \arcsin\left(\frac{\bar{v}}{V}\right) \tag{8}$$

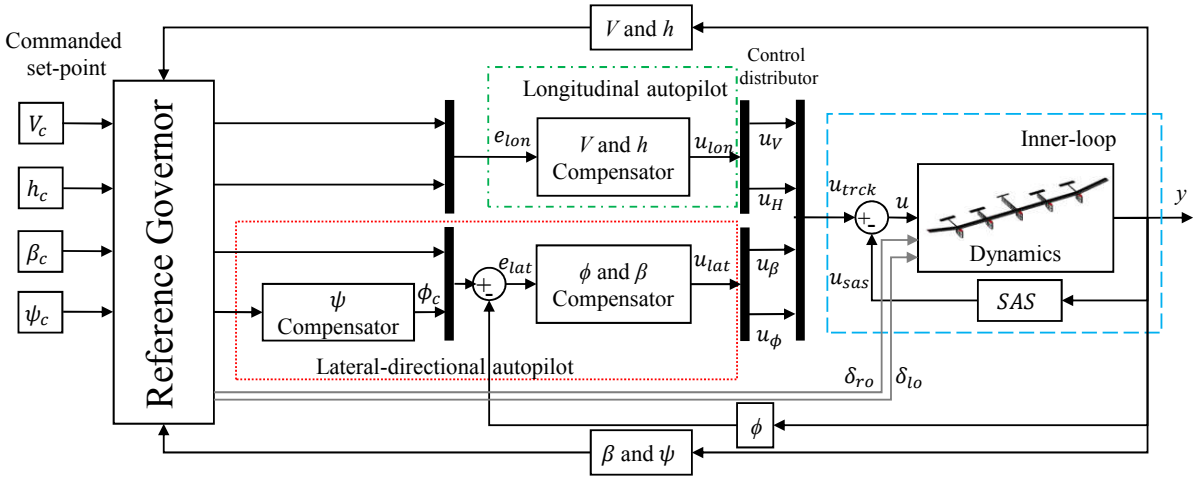

Figure 2: Control system structure.

2.1 Loop-Separation Controller

The control system designed for X-HALE is shown is Figure 2. The stability augmentation and shape control system is a proportional output-feedback controller designed to regulate the angular rates p, q, and r, In principle, this system could also regulate the deflection of the wings based on strain feedback, however, such a structural feedback is not considered in this paper. The proportional gains were calculated using a Linear Quadratic Regulator (LQR) with output feedback. The LQR allows to calculate the feedback gain matrix K by minimizing the performance index,

$$J = \frac{1}{2}\int_0^\infty (x^T Q x + u^T R u) dt. \tag{9}$$

In Eq. 9, Q is a positive semidefinite output weighting matrix and R is a positive definite control weighting matrix. The requirements of the stability augmentation system (SAS) dictate that all the poles of the closed-loop system should be placed in the left half side of the complex plane for the entire range of velocities of the aircraft. Tolerance to uncertainty was also evaluated, as the SAS must be able to ensure stability despite a 25% uncertainty in sensor measurements and control actuation [8]. The described approach results in a symmetric decoupled matrix for structural control and a decoupled matrix for stability augmentation around a trimmed level-flight condition.

The strategy of decoupling the gain matrix ensures practically desirable symmetric/anti-symmetric actuator coordination patterns that appear to result in improved closed-loop performance when deployed on the real aircraft. The closed-loop system of the inner-loop SAS based on the static output feedback, $u = -Ky$, is defined as

$$\dot{x} = (A - BKC)x = A_c x. \tag{10}$$

A standard tracker autopilot structure is used in the outer-loop. A longitudinal tracking controller for (V) and (h), and a lateral-directional tracker for β regulation and bank angle (ϕ)

tracking were developed. The ψ tracker was closed over the ϕ channel. The compensators have the form,

$$\begin{aligned} \dot{w} &= Fw + Ge, \\ u_v &= Dw + J_c e, \end{aligned} \tag{11}$$

with state (w) and output (u_v). The tracking error e is

$$e = r - z, \tag{12}$$

where r is a vector defining the references to be tracked. The matrices, F, G, D and J_c are designed to realize the desired structure in the compensator. The commands of outer- and inner-loops form the final control input,

$$u = -Ky - u_v. \tag{13}$$

The compensators for the outer-loop were optimized with the non-smooth H_∞ method which allows to address robustness and stability requirements, noise rejection and tracking requirements. The robustness requirements for the outer-loop dictate that the gain margin of all closed-loops must be higher than 6 dB and that the phase margin should be at least 45 deg. The tracker should be able to track accurately the commanded reference at the same time the controller must not react abruptly. These requirements are addressed by suitably shaping the sensitivity (S) and complementary sensitivity (T) functions. The resultant closed-loop should have high gain values for lower frequencies and low gain values for higher frequencies. Based on previous researches the bandwidth frequency of the outer-loop was set between 0.9 rad/s and 1.5 rad/s [1].

To this date, operational requirements and performance specifications for HALE aircaft have not been uniquely defined. In fact, they depend on aircraft mission which could involve high precision tasks (video surveillance) and low precision tasks (such as measuring and maintaining communications) [9]. In this paper the performance criteria are adopted that are relevant to the high precision tasks. Specifically, the altitude tracker cannot allow a steady state error greater than $\pm$ 1 m. The aircraft velocity must not deviate by more than 2% from the commanded velocity in steady state. Finally the heading angle must be maintained within 0.3 deg in steady state. These requirements are addressed via shaping of S and T functions following the process described in [1]. Nonlinear simulations results showed that an autopilot based on LSC is capable of satisfying all the performance and robustness requirements. In general, commanded references were attained with no control saturation and small tolerable steady-state errors. Nonlinear simulations showed that the autopilot is gust and performance robust, and is capable of operating under hazardous conditions and handling severe gust profiles. Nevertheless, the control approach in [1] cannot enforce flight envelope protection requirements, such as stall speed, high angles of attack or large wing deformations nor optimally account for constraints on the control surface deflections or the motor speeds, which were handled in [1] using saturation limiters. If the commanded reference is too aggressive and the maneuver is too tight, the LSC may lose the efficiency or even control of the vehicle. A reference governor is introduced in this paper as an add-on to LSC to handle constraints.

2.2 Reference Governor

The MPC-based reference governor is introduced as in [10] to modify set-point commands to the nominal closed-loop system and to directly control the elevons whenever the constraint

violation becomes imminent. The reference governor utilizes the current state vector and linear prediction model to foresee future constraint violations and, if required, modify the reference input from the desired commanded references (r_c) to the constraint-admissible reference ($\bar{r}_{c_k}$) so that the output, input and state constraints are satisfied for all present and future discrete time instants. Otherwise, the reference governor remains inactive and the nominal controller functionality is not interfered with. For example, the reference governor may smooth a step command in order to avoid large control deflections that could violate the maximum excursion of the actuator.

Consider a discrete-time linear system model which represents the inner loop system consisting of the LSC and the plant:

$$\begin{aligned} x_{k+1} &= A_r x_k + B_r \bar{r}_{c_k}, \\ y_k &= C_r x_k, \end{aligned} \tag{14}$$

where $\bar{r}_{c_k} = [\bar{V}_c \; \bar{h}_c \; \bar{\psi}_c \; \bar{\beta}_c]$ is the reference signal that is fed into the inner-loop, and the subscript r denotes quantities associated with the inner loop dynamics. Note that the vector x_k contains the aircraft states and the compensators states at time k. Let the u_{δ_o} be a vector of the left and right outer elevons control signals, which are used as extra degrees of freedom to control the wing deformation or to avoid constraint violations. To include these actuators as control inputs, columns are added to the control matrix of the inner loop system so that the discrete-time model becomes:

$$x_{k+1} = A_r x_k + \begin{bmatrix} B_r & 0 \\ 0 & B_{\delta_o} \end{bmatrix} \begin{bmatrix} \bar{r}_{c_k} \\ u_{\delta_o} \end{bmatrix} = A_r x_k + \bar{B}_r u_k^r, \tag{15}$$

where B_{δ_o} are the columns of the input matrix in Eq. 6 corresponding to u_{δ_o}. Consider the augmented vector $x_k^{\text{aug}} = [x_k^T \quad u_k^T \quad r_c^T]^T$ with dynamics given by:

$$x_{k+1}^{\text{aug}} = \begin{bmatrix} A_r & \bar{B}_r & 0 \\ 0 & I & 0 \\ 0 & 0 & I \end{bmatrix} x_k^{\text{aug}} + \begin{bmatrix} 0 \\ I \\ 0 \end{bmatrix} \Delta u_k^r = A_r^{\text{aug}} x_k^{\text{aug}} + B_r^{\text{aug}} \Delta u_k^r, \tag{16}$$

where $\Delta u_k^r = u_{k+1}^r - u_k^r$. The constrained optimization problem is then defined to achieve the tracking of the original reference signal $r_c = [V_c \; h_c \; \psi_c \; \beta_c]$, by the signal $\bar{r}_{c_k}$ subject to the imposed constraints:

$$\underset{\{\Delta u_k^r, s_{k+1}\}_{k=0}^N}{\text{minimize}} \quad J_N = \sum_{k=0}^{N-1} ||\bar{r}_{c_k} - r_c||_{Q_{r_c}}^2 + ||\Delta u_k^r||_{R_{r_c}}^2 + ||(u_{\delta_o})_k||_{R_{\delta_o}}^2 + \mu s_{k+1}^2, \tag{17}$$

subject to:

$$\begin{aligned} x_{k+1}^{\text{aug}} &= A_r^{\text{aug}} x_k^{\text{aug}} + B_r^{\text{aug}} \Delta u_k^r, && (18) \\ x_0^{\text{aug}} &= \text{current state}, \\ H_x x_k^{\text{aug}} &\leq s_k, && (19) \\ H_u u_{\delta_o} &\leq 0, && (20) \\ s_k &\geq 0, && (21) \end{aligned}$$

where Q_{r_c}, R_{r_c} and R_{δ_o} are positive definite weighting matrices, $\mu > 0$ is a weight, and N is the prediction horizon. Equations 19 and 20 represent constraints imposed on states, inputs and

outputs. The variable s_k is a slack variable used to transform state and output constraints into soft constraints in order to avoid infeasibility problems. The first term on the right-hand side of Eq. 17 is a penalty on the deviation of $\bar{r}_{c_k}$ from r_c. The second term is a penalty on the rate of change of the computed reference $\bar{r}_{c_k}$, and on the rate of deflection of the outer elevators. The third term penalizes the deflection of these control surfaces, to force them to return to the trim condition when no constraint is active, in order to reduce drag of deviations from the vehicle's nominal trajectory.

The reference governor output is defined by the first element, $\Delta r^*_{c_0}$, of the optimized reference sequence so that the reference command provided to the inner loop has the form,

$$(r_c)_{\mathrm{MPC}} = r_{c_0} + \Delta r^*_{c_0}, \tag{22}$$

where r_{c_0} denotes the previous value of r_c. Similarly, the deflection of the outer elevons is given by

$$(u_{\delta_o})_{\mathrm{MPC}} = (u_{\delta_o})_0 + (\Delta u_{\delta_o})^*_0, \tag{23}$$

where $(\Delta u_{\delta_o})^*_0$ is the first element of the optimal control increment sequence and $(u_{\delta_o})_0$ denotes the previous deflection value of the outer elevons.

Box-type constraints are imposed on the control surfaces deflections and propeller rotations, as well as on their rates. Limits are also defined for the maximum and minimum pitch angle, sideslip angle, velocities and altitude. Table 1 summarizes the constraints imposed on the input and output variables. The resultant quadratic optimization problem is convex and can be solved by existing quadratic programming solvers. The MPC controller was designed with a sampling time of 0.01 s and prediction horizon of 100 steps.

Table 1: Output and input constraints.

Description	Min	Max	Unit
Sideslip angle	-2.0	2.0	[deg]
Pitch angle	-4.0	10.0	[deg]
Forward velocity	12.5	20.0	[m/s]
Lateral velocity	-2.0	2.0	[m/s]
Altitude	0.0	120.0	[m]
Elevon deflection	-30	30	[deg]
Spoiler deflection	0	30	[deg]
Propeller rotation	3500	9000	[rpm]
Elevon deflection rate	-45	45	[deg/s]

3 RESULTS

Simulation results for four different scenarios/aircraft maneuvers are now reported. Maneuver 1 involves a heading variation, Maneuver 2 is a command in altitude, and Maneuver 3 represents a simultaneous change in altitude and heading. These simulation scenarios are used to compare the performance of the LSC and the LSC with the reference governor (LSC+RG). Finally, Maneuver 4 involves a velocity, heading and altitude change under severe wind conditions. All simulations are performed on a high fidelity simulation model of X-HALE aircraft in UM/NAST.

The results in Maneuver 1 case obtained for a commanded variation of the heading angle from 0 to 60 deg left (starting at 1 s) are presented in Fig. 3. The curves in red show simulation results without the RG, and in blue the case with the RG activated. For both simulations, all targets were reached within reasonable settling time. The final steady state errors for heading angle, velocity and altitude satisfy the requirements. However, without the RG, the maximum sideslip angle constraint is violated in transients. With the RG, sideslip angle is maintained within the prescribed limits, while the outer elevons are used to assist during the maneuver and help avoid constraint violations. Note that, the spoilers direct the aircraft to the left by deflecting the left control surface. When the RG predicts that the sideslip angle constraint is going to be violated, the right outer elevon deflects downwards an the left outer elevon deflects upwards(Fig 3). [1] and [11] showed that asymmetrical deflections in control surfaces installed far from the wing's elastic axis induce torsion on the wing. The deflection of the elevons observed in the first 2 s of the maneuver reduces the angle of attack of the right half-wing with respect to the left half-wing due to the torsion of the wing box. This change in the wing loading keeps the aircraft response within the specified constraints. It also reduces the oscillations of the structure, and, in particular, the LSC+RG controller has a lower downward deformation. Fig. 3 bottom right shows left and right wingtips dynamics using both controllers.

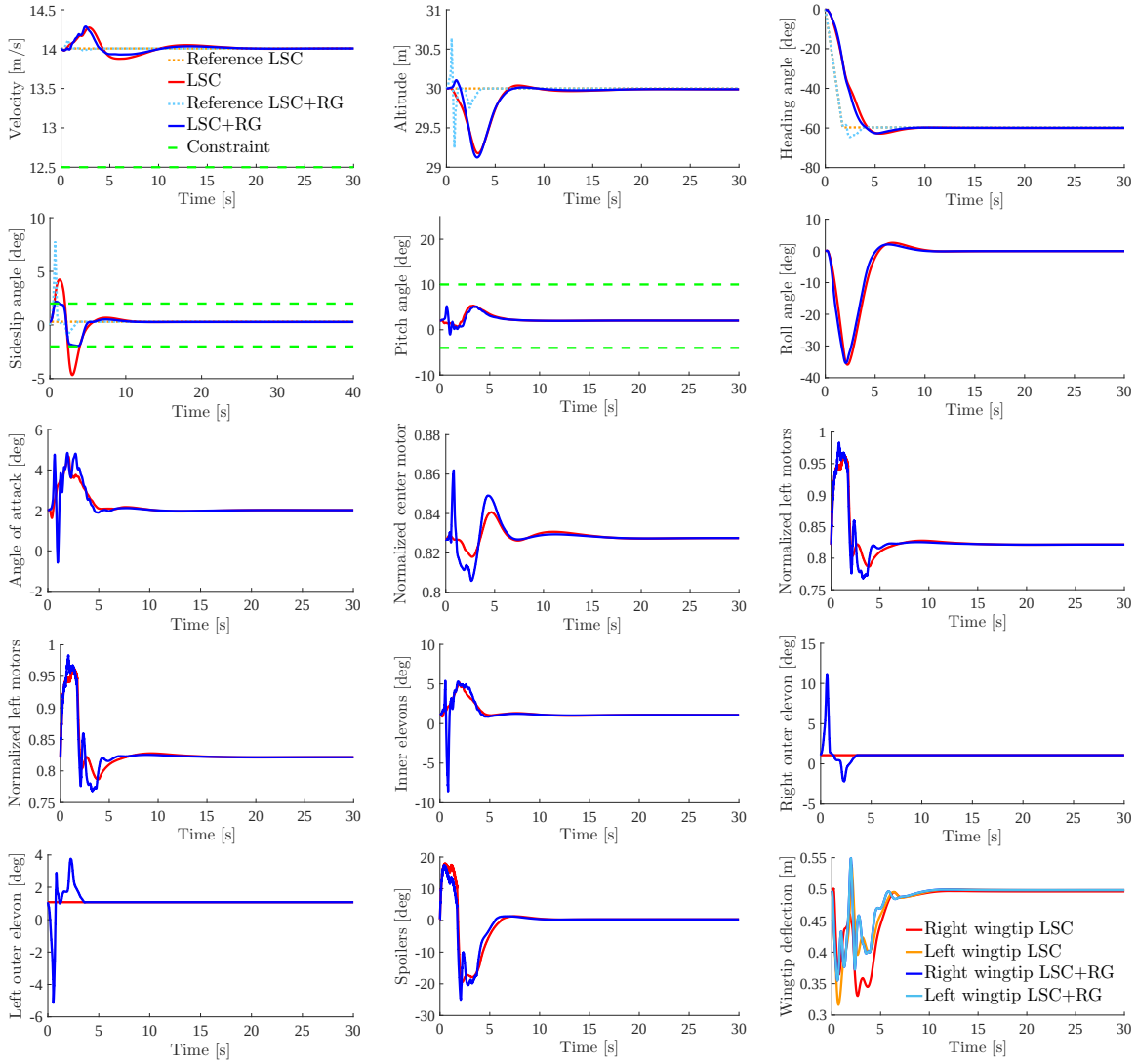

Figure 3: X-HALE response time histories due to commanded heading angle variation.

In the second simulated maneuver, an altitude variation from 30 m to 38 m was commanded, while all the other references were kept constant. The objective was to follow such an altitude change while maintaining the heading and sideslip angles close to zero. Figure 4 shows the nonlinear simulation results. The maneuver was accomplished successfully in both cases LSC and LSC+RG. Note that there was no constraint violation for the LSC+RG controller. However, the LSC without RG violates the pitch angle limit, with the maximum pitch angle excursion of 21.56 deg versus the limit of 10 deg. To avoid the violation of this constraint, the RG commands the outer-elevons to deflect, this induces a roll, but allows reducing and holding the pitch angle. As the pitch angle constraint is imposed as a soft constraint, a slight constraint violation (within 0.5 deg) occurs for LSC+RG case. The motors saturate for the LSC but not for the LSC+RG. In fact, in the LSC+RG case, the control signals remain within their limits. The improved control of the pitch angle without large excursions in LSC+RG case allows to maintain a constant rate of climb and avoids larger structural deflections. In particular, LSC controlled aircraft deflects the wingtip up to 0.75 m, which is 8.5% higher with respect to the LSC+RG controlled aircraft.

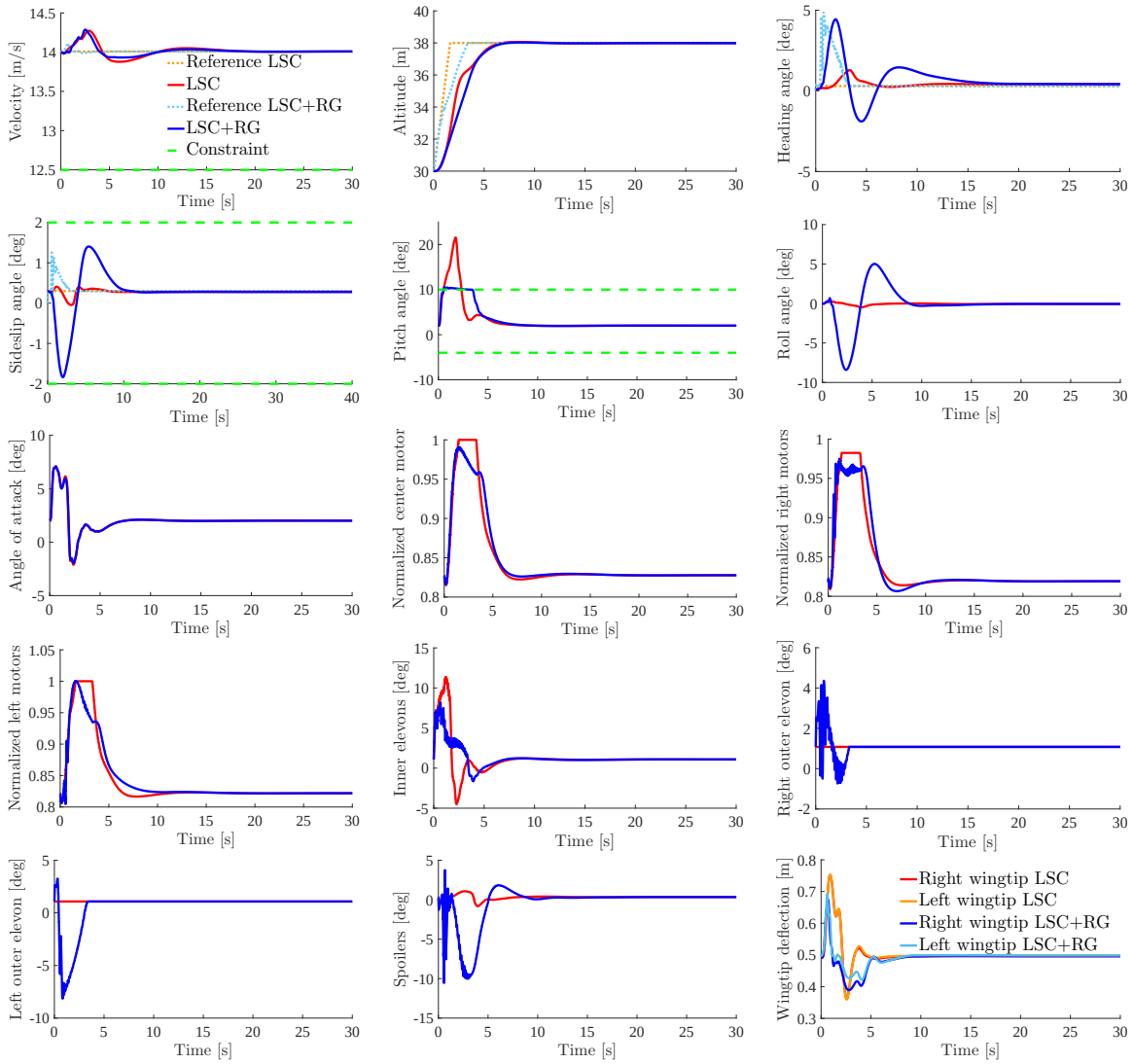

Figure 4: X-HALE response time histories due to commanded altitude variation for Maneuver 2.

Maneuver 3 is a tight and aggressive maneuver in which the aircraft is commanded to turn and increase altitude at the same time. More specifically, the commanded altitude is 38 m

and the commanded turn is 45 deg left. Figure 5 presents the nonlinear simulation results for Maneuver 3. The LSC+RG controller successfully takes the aircraft to the commanded altitude and heading with the steady state errors well within the specified limits. Note that the constraints for pitch and sideslip angle become active during the maneuver. The outer elevons acted to hold the constrained values within limits and the RG modified the commanded reference. All control surfaces as well as the central and right motors were far from saturation. The only saturated actuators were the left motors. The RG took this into account and adjusted the commanded reference accordingly. The LSC without RG failed to control the aircraft and the simulation diverged after 2.8 s (Fig. 5). While the LSC is able to track commands in multiple channels [1], the difference in this case is the aggressiveness of the maneuver. The command is so swift that the controllers act almost immediately to track the reference. However, the linear controller is not able to foresee the saturation of the motors nor the effect of such an aggressive deflection of the inner elevons to attain the commanded altitude while it keeps the velocity constant. The effect of increasing the angle of the inner elevons without enough power in the motors results in a sudden reduction in the airplane pitch angle. The lack of structural regulation is also a problem in this case. Once the aircraft starts pitching down, the inertial effects make the wing tips deflect downward from 0.577 to -0.172 m in less than 0.5 s. The result, loss of control, is catastrophic for the simulated aircraft.

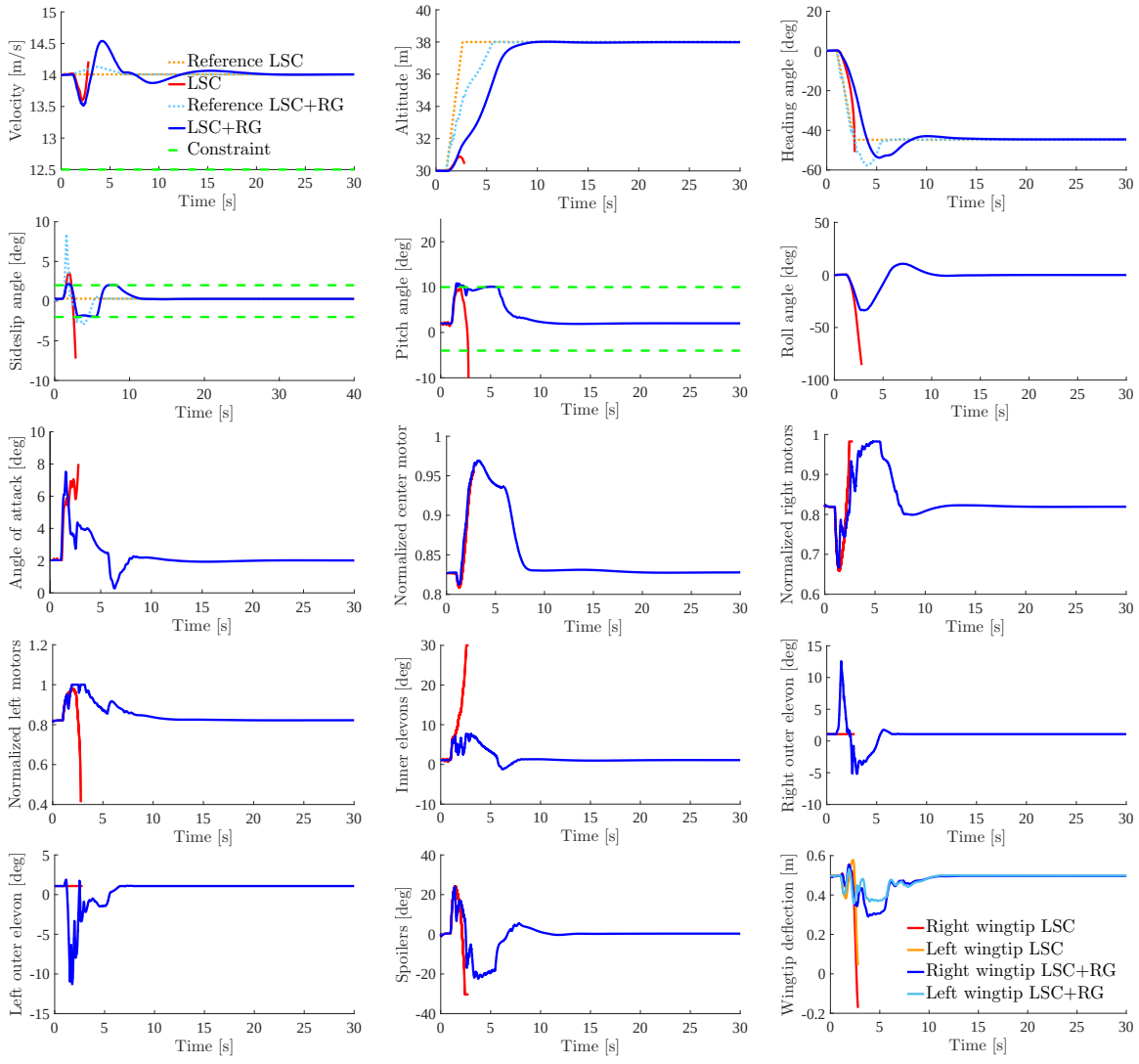

Figure 5: X-HALE response time histories due to commanded altitude and heading variation for Maneuver 3.

These simulations show the advantage combining LSC and RG. Some commanded references could induce a linear controller to develop control signals that are dangerous to the aircraft. Under different commands (smoother references) the LSC without structural feedback operates satisfactorily and allows the aircraft to accomplish the maneuvers for a usual X-HALE mission profile, with and without gusts. However, if an emergency situation or a mission requires more aggressive commands, the controller without protection for constraint violation can induce the aircraft to the condition shown in Fig. 5.

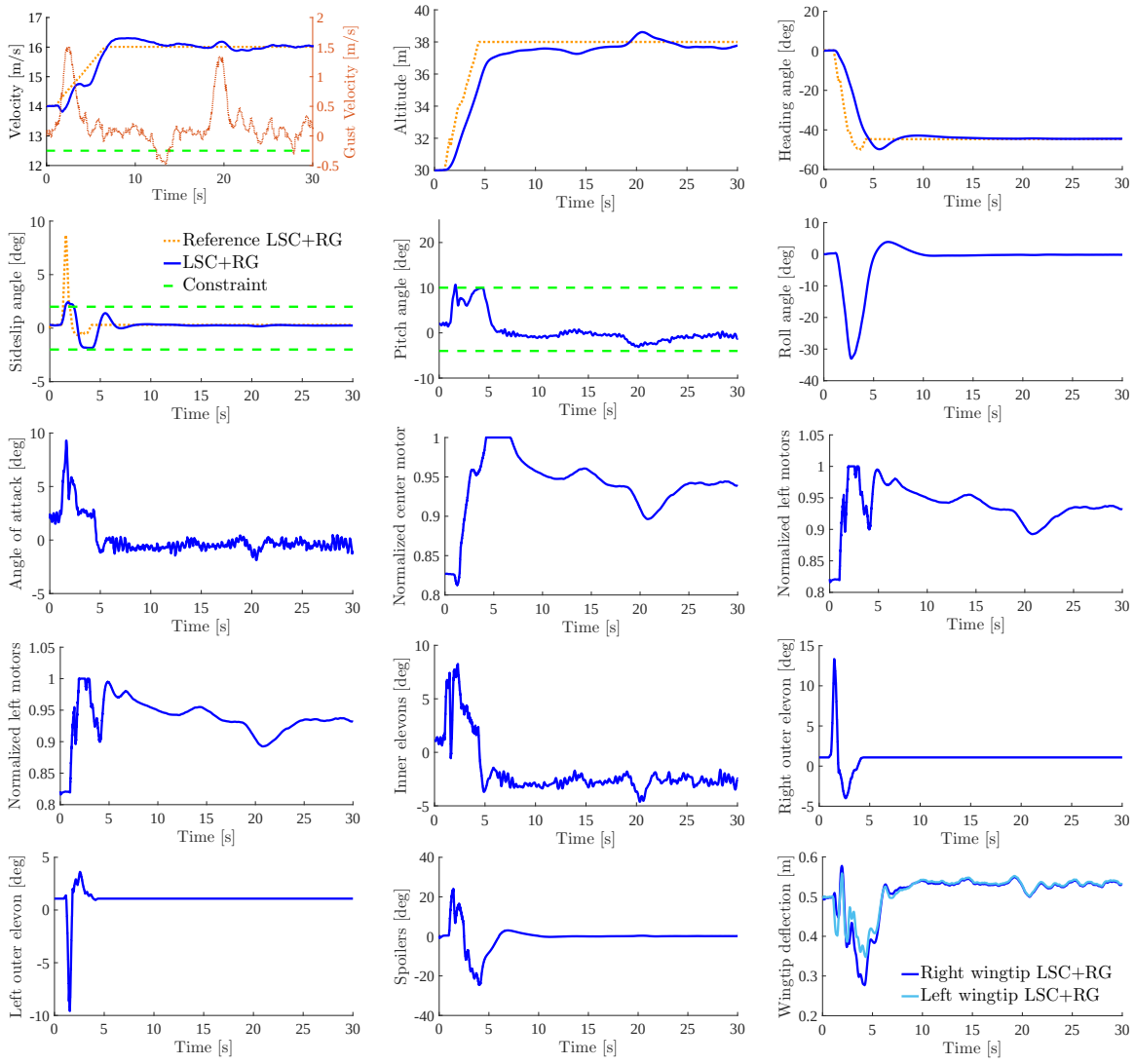

Figure 6: X-HALE response time histories due to commanded altitude, velocity and heading under severe wind conditions (Maneuver 4).

To evaluate the performance and the robustness of the LSC+RG controller, a gust profile was applied in the fourth simulation scenario, which is representative of the most extreme wind condition that X-HALE was designed to operate. Figure 6 shows the X-HALE nonlinear response and variation of control inputs for Maneuver 4 under wind condition. The controller must track references in velocity, heading and altitude at the same time while regulating the sideslip angle. Departing from the trim condition, the vehicle is commanded to change its altitude to 38 m while turning 45 deg left and increasing its velocity to 16 m/s. The gust profile consists of two 1-cos 1.34 m/s gust (3 mph from the aircraft test cards) plus a von Karman profile. The gust velocity over the von Karman profile varies between ± 0.5 m/s. The final gust profile is shown

in the right axis of the velocity plot (Fig. 6).

All the commanded references are reached and tracked within the specified tolerances. The LSC is robust enough to handle variation in velocity, altitude and heading under hazardous wind conditions. The velocity overshoot is 0.29 m/s and the final steady state velocity oscillates around the commanded reference with acceptable deviations. The heading angle exhibits an overshoot of 5.26 deg, this overshoot is compensated by the spoilers to make the aircraft attain the commanded heading of 45 deg. The final altitude is also regulated around the commanded altitude of 38 m. The sideslip and pitch angle constraints become active in transients. All motors reach maximum throttle, and the outer elevons are activated to protect aircraft against violating the limits. Once the aircraft reaches the steady state condition, the outer elevons are no longer activated. Due to constraints imposed as soft and the effects of gust, the sideslip and pitch angle limits are slightly violated, but nonetheless these small violations are acceptable in practice.

4 CONCLUSION

A flight control system for a very flexible aircraft based on the combination of the Loop Separation Controller (LSC) and a reference governor (RG) has been proposed. The LSC is able to control the vehicle and satisfy nominal performance and robustness requirements. However, nonlinear simulation results revealed that aggressive commands can lead to violations of the performance requirements and aircraft loss of control. The RG is able to manage the reference commands to satisfy the performance requirements and keep the aircraft safe. The use of reference governors to handle aircraft limits and protect the flight envelope avoids the aircraft from entering a flight condition that may compromise its operation.

The use of the RG to augment the LSC in the inner-loop controller offers an advantage over pure MPC solutions, since the LSC can be tuned and tested using conventional tools. All performance and robustness requirements, in particular, in frequency domain can be ensured before the RG is augmented to protect the system against constraint violation. This "augment rather than replace" approach can facilitate fulfilling formal certification requirements for predictive controllers in very flexible aircraft. From broader perspective, augmenting an MPC controller to a well-tuned and previously tested inner-loop controller is promising as the closed-loop response models can be simpler than open-loop response models, while tuning and calibration of the MPC controller on an experimental system entails less risk.

5 REFERENCES

[1] González, P. J., Guimarães, A. B., Bertolin, R., Silvestre, F. J., and Cesnik, C. E. S. (2017). X-HALE autopilot with stability augmentation and shape control based on loop separation. In *International Forum on Aeroelasticity and Structural Dynamics*. IFASD 2017-77, Como, Italy.

[2] González, P. J., Silvestre, F. J., Paglione, P., Köthe, A., Pang, Z. Y., and Cesnik, C. E. S. (2016). Linear control of highly flexible aircraft based on loop separation. In *Atmospheric Flight Mechanics Conference*. AIAA 2016-3398, Washington DC.

[3] Apkarian, P. and Noll, D. (2006). Nonsmooth H_∞ Synthesis. *IEEE Transactions on Automatic Control*, 51(1), 71–86.

[4] Garone, E., Di Cairano, S., and Kolmanovsky, I. (2017). Reference and command governors for systems with constraints: A survey on theory and applications. *Automatica*, 75(1), 306–328.

[5] Shearer, C. M. and Cesnik, C. E. S. (2007). Nonlinear flight dynamics of very flexible aircraft. *Journal of Aircraft*, 44(5), 1528–1545.

[6] Su, W. and Cesnik, C. E. S. (2011). Dynamic response of highly flexible flying wings. *AIAA Journal*, 49(2), 324–339.

[7] Cesnik, C. E. S., Senatore, P. J., Su, W., Atkins, E. M., and Shearer, C. M. (2012). X-HALE: A very flexible unmanned aerial vehicle for nonlinear aeroelastic tests. *AIAA Journal*, 50(12), 2820–2833.

[8] Rona, F., González, P. J., Silvestre, F. J., Cesnik, C. E. S., and Pang, Z. Y. (2018). Robustness analysis of a stability augmentation system of a highly flexible aircraft. In *2018 AIAA Guidance, Navigation, and Control Conference*. AIAA 2018-0604, Kissimmee, Florida.

[9] USAF (1975). Military specification: Flight control systems general specifications for design, installation, and test of piloted aircraft. *MIL-F-9490D*.

[10] Virgilio Pereira, M. F., Kolmanovsky, I., Cesnik, C. E. S., and Vetrano, F. (2019). Model predictive architectures for maneuver load alleviation in very flexible aircraft. In *2019 Scitech Forum*. AIAA 2019-1591, San Diego, California.

[11] Guimarães, A. B., Silvestre, F. J., Bussamra, F., Silva, R. G., and Cesnik, C. E. S. (2017). Response and stability of the remotely-piloted, constrained X-HALE aircraft in wind tunnel. In *International Forum on Aeroelasticity and Structural Dynamics*. IFASD 2017-81, Como, Italy.

COPYRIGHT STATEMENT